# The effect of low temperature heat treatment on surface chemistry and corrosion resistance of commercial magnesium alloys AZ31 and AZ61 in 0.6 M NaCl solution.

Sebastián Feliu (Jr)[a] , Alejandro Samaniego, Violeta Barranco, A.A. El-Hadad, Irene Llorente.

[a]Centro Nacional de Investigaciones Metalúrgicas CSIC, Avda. Gregorio del Amo 8, 28040 Madrid, Spain, (e-mail: sfeliu@cenim.csic.es), (e-mail: jcgalvan@cenim.csic.es)

[c]Instituto de Ciencias de Materiales de Madrid, ICMM, Consejo Superior de Investigaciones Científicas, CSIC, Sor Juana Inés de la Cruz, 3, Cantoblanco, 28049, Madrid, Spain

Corresponding author: Tel.: +34 91 5538900. Fax.: +34 91 5347425. E-mail address: sfeliu@cenim.csic.es

**Abstract:** This paper studies the differences in chemical composition of the oxide surface layers induced by heating in air at 200ºC for time intervals from 5 minutes up to 60 minutes on commercial AZ31 and AZ61 magnesium alloys with a view to a better understanding of their protective properties. A strong link was found between the aluminium enrichment observed in the surface of the oxide layer and the decrease in the protective properties of the heat treated AZ31 alloy. In contrast, no significant changes have been observed in the case of the heat treated AZ61 alloy.

**Keywords**: A. Magnesium; B. XPS; B. SEM; C. Passivity; C. Segregation.

## 1. Introduction

The chosen study materials are Mg-Al alloys, which have aroused great scientific and technological interest over the last two decades. From a practical point of view magnesium is the structural metal of lowest density, which makes it highly attractive for use in the automotive, aerospace, IT and electronics industries, where weight plays a decisive role. However, as magnesium is one of the chemically most active metals, insufficient resistance to atmospheric and aqueous corrosion sometimes limits its applications. Thus it is desirable to have as complete as possible information on the factors that influence the corrosion of these materials. This work seeks to contribute to such information.

Many researchers have carried out studies to find relationships between changes in the alloy microstructure (amount and distribution of β-phase precipitates) with long term heat treatments (T4 (solution treatment) or T6 (aging treatment)) [1-10] and changes in corrosion resistance. In the literature a great deal of attention has been paid to the role of the β-phase in the corrosion mechanism of magnesium/aluminium alloys. A generally accepted idea is that this phase acts as an effective cathode and/or barrier against corrosion, depending on its size and distribution [1].

Oxide film formation and properties like protectiveness may be sensitive to the conditions in which the film grows. Laboratory tests normally refer to the behaviour of surfaces that have been mechanically polished prior to testing in order for metallographic observation and to remove the impurities and oxidation/corrosion product layers formed during the manufacturing and subsequent storage of the alloy. However, it is of particular technological

interest to obtain information on the chemical composition of the surface in as-received condition (untreated surface), because these alloys are normally used with most of the surface intact and the cost of polishing treatment limits its industrial application [11]. The literature contains controversial views relating to the effect of skin characteristics on the corrosion performance of magnesium alloys [11]. Song et al. [12] reported that the skin of die cast AZ91D showed better corrosion resistance than the interior. The opposite conclusion was obtained by Yu and Uan [13] and Zhang et al [14]. Recently, Song and Xu [15] have observed an improvement in the corrosion performance of AZ31B Mg alloy sheet by surface polishing.

In a previous study [16], XPS analysis revealed notable differences in the chemical composition, structure and thickness of the external oxide films on the surface of AZ31 and AZ61 alloys in as-received and freshly polished conditions. In the joint analysis of XPS and EIS data, attention was drawn to the significant decrease in the corrosion resistance value of the alloys in as-received conditions In immersion test in saline solution, during the initial stages of testing, considerable higher corrosion rates were obtained in as-received specimens compared to the freshly polished surfaces. The formation of an additional thin (thickness of just a few nanometres) and non-uniform external oxide layer (in the form of islands) composed by a mixture of spinel ($MgAl_2O_4$) and MgO as a result of the manufacturing process seemed to diminish the protective properties compared to the more perfect and uniform films formed on freshly polished surface. An economic and simple method to generate on a material a protective barrier against the effects of aggressive environments is to expose it to a thermal treatment in an oxygen rich atmosphere [17]. Following

up the idea that the initial external oxide film plays an important role in the resistance to magnesium corrosion initiation and its propagation [1,16,18], in the present research it is studied the possibility of improving its protective properties by short time low temperature heat treatments in air.

From a scientific point of view, Jeurgens et al. [19] noted that the thermal oxidation of metallic alloys at low temperatures (e.g. at T < 600 K) and for short times has only scarcely been investigated. The detailed chemical composition and constitution of the oxide films formed on such alloy surfaces at low temperatures for short heating times are unknown and there is no comprehensive knowledge of the effect of the concurrent processes of chemical segregation and preferential oxidation on the developing oxide-film.

Czerwinski [20] studied the oxidation behaviour of AZ91D Mg alloy at different temperatures. The results showed that AZ91D exhibited protective oxidation only at a temperature of 197ºC, while at higher temperatures the behaviour was non-protective and associated with the formation of oxide nodules and their coalescence into a loose fine-grained structure. On the basis of these results, we have selected a low-temperature heat treatment process at 200ºC to study the possibility of improving the protective properties of the external oxide film on the surface of AZ31 and AZ61 Mg alloy in as-received condition.

Thus, special objective of this research is to study the effect of the type of alloy and heating time at 200ºC on the chemistry of the outer thin films formed on the surface of magnesium alloys after short heat treatments and their corrosion resistance in saline solution.

## 2. Experimental

The chemical compositions of the tested magnesium alloys, AZ31 and AZ61, are listed in Table 1. They were fabricated in wrought condition and supplied in 3 mm thick plates by Magnesium Elecktron Ltd, UK, Manchester. This research compares the behaviour of specimens of the above alloys in the two following surface conditions: specimens in as-received condition, which means that the surface of the samples was untreated and had only been cleaned with distilled water and dried with hot air, and freshly polished specimens, which were dry ground with successive grades of silicon carbide abrasive paper from P600 to P2000 followed by finishing with 3 and 1 μm diamond paste, cleaned in water and dried with hot air. The following nomenclature is used in the remainder of the paper to designate the four dual combinations tested: AZ31-O, AZ31-P, AZ61-O, and AZ61-P, where the letters O and P, that accompany the alloy type, denote: O = original surface condition (i.e. as-received); P = polished surface condition.

The two alloys were oxidised in identical conditions in a thermogravimetric analyser (TGA) (TA instruments Q600 SDT) using cylindrical specimens of 4 mm in diameter by 2 mm in height (weight approximately 100 mg). The apparatus was capable of accommodating a specimen with a maximum weight of 0.5 g and had a measurement accuracy of 0.1 μg. The reaction temperature was monitored by a Pt/Pt–Rh thermocouple. Weight change kinetics were measured in air under isothermal conditions at a temperature of 200°C. The heating rate before reaching the isothermal condition was 50°C/min. For reference, thermogravimetric measurements of weight change versus time are also shown for freshly polished AZ31 and AZ61 alloys in an air environment. In

this case, the as-received specimens were dry ground through successive grades of silicon carbide abrasive papers from P600 to P2000 followed by finishing with 3 and 1 μm diamond paste, rinsing in water and drying with hot air.

The thermal treatment was very simple, consisting of the horizontal exposure of 2 cm x 2 cm square specimens of the AZ31 and AZ61 alloys in a convective stove at 200°C in air for 5, 20 and 60 minutes.

The tested specimens were examined by scanning electron microscopy (SEM) using a JEOL JXA 840A unit operating with Rontec EDR288 software for EDX spectra acquisition and image digitalisation.

Photoelectron spectra were recorded using a Fisons MT500 spectrometer equipped with a hemispherical electron analyser (CLAM 2) and an Mg Kα X-ray source operated at 300 W. The specimens were fixed on small flat discs supported on an XYZ manipulator placed in the analysis chamber. The residual pressure in this ion-pumped analysis chamber was maintained below $10^{-8}$ torr during data acquisition. Spectra were collected for 20-90 min, depending on the peak intensities, at a pass energy of 20 eV, which is typical of high-resolution conditions. The intensities were estimated by calculating the area under each peak after smoothing and subtraction of the S-shaped background and fitting the experimental curve to a combination of Lorentzian and Gaussian lines of variable proportions. Although specimen charging was observed, it was possible to determine accurate binding energies (BEs) by referencing to the adventitious C 1s peak at 285.0 eV. The atomic ratios were computed from the peak intensity ratios and reported atomic sensitivity factors [21]. The

measurements were performed at take-off angles of 45° with respect to the specimen surface. The sampled areas were 1 x 1 $mm^2$.

Electrochemical impedance measurements were conducted in 0.6 M NaCl after 1 hour, 1 day, 7, 14, 21 and 28 days of exposure at room temperature (25°C). An AUTOLAB potentiostat, model PGSTAT30, with frequency response analyser (FRA) software was used. The frequency ranged from 100 kHz to 1 mHz with 5 points/decade, whereas the amplitude of the sinusoidal potential signal was 10 mV with respect to the open circuit potential. A typical three-electrode set-up was employed: Ag/AgCl and graphite were used as reference and counter electrodes, respectively, and the material under study was the working electrode.

Also, the corrosion of the magnesium alloys was estimated by determining the volume of hydrogen evolved during the corrosion process. Samples for hydrogen gas collection were cut into square coupons with dimensions of 2 cm × 2 cm x 0.3 cm and horizontally immersed in 700 ml of quiescent test for 11 days in a beaker open to laboratory air at 20 ± 2 °C. The hydrogen evolved during the corrosion experiment was collected in a burette by a funnel above the corroding sample, as described by Song et al [12, 22, 23]. The experiments were run simultaneously and each sample was subjected to essentially the same temperature and exposure history.

The morphology of the attack on the corroded surface was examined at low magnification and a camera was used to take the photographic images. Once the test was finished, the corroded specimens were were pickled in chromic acid

to remove the corrosion products, then rinsed with isopropyl alcohol and dried in hot air in order to study the corrosion morphology

## 3. Results

### *3.1. Thermogravimetric analysis*

Figure 1 compares the evolution in weight gain values with heating time at 200°C in air on the AZ31-O, AZ31-P, AZ61-O and AZ61-P specimens. AZ31-O specimen presents a linear increase in weight gain values with time, whereas AZ61-O specimen shows a strong decrease in weight gain values, which are approximately 4 times lower at the end of the test (60 min) than the corresponding values for the AZ31-O specimen (Fig. 1). In contrast to the great differences observed between the AZ31-O and AZ61-O specimens, it is interesting to note the very similar weight gain values found for the AZ31-P and AZ61-P specimens (Fig. 1).

### *3.2. Morphology and microcomposition of the oxide layer formed on the surface of the AZ31 and AZ61 magnesium alloys after the heat treatment for different times.*

Figure 2 compares the surface morphologies on the non-heated and heated for different times AZ31-O and AZ61-O specimens. As can be seen, the metallic surface of the non-heated AZ31-O specimen appears to be covered by a large number of white precipitated particles (Fig. 2a), whereas in the surface of the non-heated AZ61-O these particles are not apparently visible (Fig. 2b). After 5 minutes of the heat treatment, attention is drawn to the significant presence of black zones on the surface of the oxide layer formed on the AZ61-O specimen (as marked by circles in Fig. 2d). In contrast, these black zones are hardly observed on the surface of the oxide layer formed on the AZ31-O specimen (Fig. 2c). By comparing Fig. 2d with Fig 2f and 2h for the AZ61-O specimen, it is

apparent that the fraction of the surface covered by the black zones decreases gradually with the heating time.

EDX analysis of the AZ31-O specimen surface after heating for 60 minutes was performed for points labelled in Fig. 3 in order to investigate possible differences in composition between the white precipitated particles and the larger darker regions associated with the α-Mg matrix. Atomic percentages and Al/(Al+Mg)x100 ratios of the white particles obtained by EDX are presented in Table 2 and compared with the measurements made in the darker regions. In EDX analyses obtained on the white particles, attention is drawn to the increase in the Al, Zn and Mn content and the decrease in the Mg content compared to the darker regions.

Fig. 4 compares the variation in the Al/(Al+Mg) x 100 atomic ratio of the darker regions obtained by EDX on the surface of the AZ31-O and AZ61-O specimens as a function of the heating time

*3.2. Changes in the chemistry of thermally oxidised films formed on AZ31 and AZ61 alloys in as-received condition with heating time*

Figure 5 compares the atomic percentages of O, Mg, Al and Zn obtained by XPS on the surface of the AZ31-O and AZ61-O specimens and their variation with heating time.

Figure 6 compares the Al/(Al-Mg) x 100 atomic ratios obtained by XPS on the surface of the non-heated AZ31-O and AZ61-O specimens with those resulting from the heat treatment at a temperature of 200°C for different times. The

Al/(Mg+Al) x 100 ratio determined by XPS is about 11 for the non-heated AZ31-O specimen surface (Fig. 6), which is much higher than the 3% content in the bulk alloys (Table 1). Heat treatment times of 60 minutes promotes an increase in this ratio on the surface of the AZ31-O specimen (Fig. 6). On the other hand, an important decrease is detected in the Al/(Mg+Al) x 100 ratio in the surface of the AZ61-O specimen heated for 5 minutes (Fig. 6), which suggests the preferential growth of a magnesium-rich film (magnesium oxides or hydroxides) that covers the non-heated surface. Longer heating times (20 and 60 minutes) lead to an increase in the Al/(Mg+Al) x 100 ratio on the AZ61-O (Fig. 6) that may be related with the enrichment in Al of the outer oxide layer formed at the shortest heating times. This significant aluminium enrichments detected by XPS on the surface of the AZ61-O specimen heated for 20 and 60 minutes respect to the AZ61-O specimen heated for 5 minutes (Fig. 6) are consistent with the decrease in the fraction of the surface covered by the black zones observed by SEM (Figs. 2d, 2f and 2h). In contrast, it is interesting to note the absence of significant variations of the Al/(Al+Mg) ratios detected by EDX in the oxide layer formed on the surface of the AZ61-O specimens with the heating time (Fig.4). It is worth mentioning that, while XPS gives the composition information of the very top surface oxide layer (thicknesses of only few nanometers), EDX gives information of the bulk of this layer (thicknesses of several micrometers).

Figure 7 shows the O1s (a) Mg 2p (b) Al 2s (c) and $Zn2p_{3/2}$ (d) XPS high resolution spectra obtained on the surface of the AZ31-O specimen after 5 minutes of heating. These spectra are representative of the similar spectra obtained on the surface of non-heated AZ31 and AZ61 alloys and after other heating times. The O1s spectrum (Fig. 7a) show the most intense component at

a binding energy of 531.2 eV, associated to the presence of oxygen in the form of magnesium oxide, MgO [24-26], and another less intense component at a binding energy of 533.2 eV, which may be attributed to the presence of oxygen in magnesium hydroxide or $Al(OH)_3$.[27]. The Mg 2p spectrum (Fig. 7b) presents one single component associated to the presence of magnesium in the form of magnesium oxide or hydroxide (51.0 eV). [28, 29]. The Al 2s spectrum (Fig. 7c) may be fitted to one component at 119.5 eV due to the presence of $Al^{3+}$. Finally, The $Zn2p_{3/2}$ high resolution spectrum (Fig. 7d) may be fitted to one component with a binding energy of 1022.0 eV associated with the presence of $Zn^{2+}$.

*3.3. Electrochemical impedance measurements*

The evolution of the corrosion process of the heat treated AZ31-O and AZ61-O specimens has been monitored by means of impedance measurements with the specimens immersed in 0.6 M NaCl solution. Nyquist diagrams (Figs. 8) show the presence of a capacitive loop at high frequencies (HF). In the literature about the corrosion of magnesium alloys is normal to associate the diameter of this capacitive loop with the charge transfer resistance ($R_t$) of the corrosion process [30-32], value which is inversely related to the corrosion current ($i_{corr}$) through the Stern-Geary equation [33]:

$$I_{corr} = B/ R_t \qquad (1)$$

B being a constant. Empirical determinations of constant B for the experimental conditions of this study has yielded values of about 65 mV for the AZ31 alloy and 120 mV for the AZ61 alloy, values used in the calculations.

Fig. 9 shows the evolution of the $R_t$ values deduced from the capacitive loop at high frequencies in function of immersion time in 0.6M NaCl solution. $R_t$ data together with equation (1) have enabled electrochemical calculations of corrosion rate. This way, the results depicted in Fig. 10 were determined, which show the corrosion rate variations with time over 28 days immersion. Taking the values for the non-heated or heated for 5 minutes AZ31-O specimens as reference, heat treatment for 20 and 60 minutes increases markedly the corrosion rate values (Fig. 10 a), while in the case of AZ61-O specimens (Fig. 10b), little effect or a moderate decrease in the corrosion rate is observed. Fig. 11 is instructive in showing the differences in the hydrogen volume data between alloys AZ31 and AZ61 over 7 days of immersion in 0.6 M NaCl. It is interesting to note that similar trends regarding the corrosion behaviour are deduced from these hydrogen evolution that from the electrochemical ones.

Fig. 12 compares the macroscopic surface appearance of the corroded non-heated and heated for 60 minutes AZ31-O specimens after 7 days of immersion in NaCl 0.6M and after corrosion product removal. In the test samples one can observe uniform attack on large areas of the exposed surface of the non-heated AZ31-O specimen (Fig. 12a). However, after 60 minutes (Fig. 12b) of heat treatment, some wide pits seem to cover the specimen surface. In general, there is a qualitative agreement between the presence or absence of pits on the surface of the corroded specimens (Fig. 12) and the corrosion data (Fig. 11a).

## 4. Discussion

*4.1. Changes in chemical composition of the oxide layers grown on the surface of AZ31 and AZ61 alloys in as-received condition after heat treatment at 200°C*

Figure 1 shows that the polished AZ31 and AZ61 specimens present much lower increases in weight gain during heat treatment than the corresponding specimens in the as-received surface condition. As can be seen in figure 1, 35-60 minutes of heating at 200ºC produces a very small weight gain, around only 0.6 µg/cm$^2$, which is similar for the two alloys. It is generally accepted that the growth of compact MgO films is controlled by solid sate diffusion through adherent oxide areas followed by the reaction with oxygen at the oxide/gas interface, hence a lack of easy-paths for fast Mg transport could be a possible explanation for a highly protective behaviour [20]. From Eq. (2) [34]:

$D_L = 1.0 \times 10^{-6} \exp( - 150000/ RT)$ m$^2$ / s (2)

Diffusivity ($D_L$) of Mg within the MgO lattice at 473 K is as low as 2.67 x 10$^{-23}$ m$^2$/s justifying negligible weight gains.

This behavior is not detected in the case of the AZ31-O and AZ61-O specimens (Fig. 1) which tends to suggest that the increase in weight gain with the heat treatment is dependent of the initial surface condition of the studied alloys. As Table 3 shows, roughness values of the AZ31-O and AZ61-O specimens are more than ten times greater than for the AZ31-P and AZ61-P specimens. Nanometric scale details of the typical surface roughness exhibited by the tested specimens are given in Fig 13. The difference in weight gain with heating time between the as-received and polished surfaces (Fig. 1) may be in

agreement with the very heterogeneous and likely defective surface layer present on the as-received surfaces (Fig. 13) compared to the continuity of the oxide films formed on the polished specimens. Similarly, in previous work [16, 18, 35] with the same alloys in 0.6M NaCl saline solution, an inhibiting effect of the homogeneous and continuous native oxide surface film formed on freshly polished samples was observed.

One point emerging from the set of the weight gain values (Fig. 1) is the clear tendency for AZ31-O specimen to present higher values than the AZ61-O specimen throughout the heat treatment.

It is important to note the close relationships between the difference in increases in weight gain values with heating time for AZ31-O and AZ61-O specimens and the differences in chemical composition observed by XPS and EDX in the oxide films formed on the surface of these alloys during heat treatment. Thus, figure 1 shows a very significant increase in the weight gain values and the EDX (Fig.4) and the XPS data (Fig.6) indicates an increase in the aluminium contents, while for the AZ61 alloy the increase in weight gain values is relatively small (Fig. 1) and only a slight increase in aluminium is detected on its surface (Figs. 4 and 6).This relationship appears to suggest that some common factor is acting on the mechanisms that determine both magnitudes. One immediate idea is that they may be directly related with the ease of diffusion of aluminium atoms towards the aforementioned surface. Moreau et al [36] have found that the volume diffusion coefficient for aluminium in magnesium can be determined using:

$$D_L = 3.39 \times 10^{-4} \exp( - 135000/ RT) \ m^2 / s \quad (3)$$

which gives a value of 4.112 x $10^{-19}$ $m^2$/s at 200ºC. On the other hand, diffusivity of Al in the grain boundaries of the magnesium alloys is as high as 9.263 x10 $^{-12}$ $m^2$/s at 200ºC [37]. The obtained values show that the volume diffusion coefficient is approximately 7 orders of magnitude less than the diffusion coefficient for the grain boundary. At 200ºC the process of Al surface segregation is controlled by grain boundary diffusion.

The microstructure of the non-heated AZ31 alloy is formed practically by an α matrix with Al in solid solution surrounded by grain boundary free of precipitates of β phase (Fig.14a). In contrast, the aluminium is distributed, forming part of the chemical composition of the β-phase precipitates in the grain boundary of the AZ61 alloy (Fig.14b). Available literature [38, 39] mentions that the presence of stable intermetallics at the grain boundary reduces the activity of atom diffusion along the grain boundary. It is likely that blockage of the grain boundaries in the AZ61 alloy due to preferential precipitation of β phase inhibits the diffusion of aluminium solute along the grain boundary of the magnesium matrix at 200ºC compared to the AZ31 alloy. Also, this can probably explain the initial presence of the called" white spots" with high Al content on the surface of the AZ31-O specimen as a result of the manufacturing process and their absence on the AZ61-O specimen (Fig. 2).

The EDX (Fig.4) and XPS analyses (Fig.6) suggests a considerable superficial aluminium species enrichment of an AZ31 alloy that has been heat treated. This is surprising since the magnesium content in the bulk alloy is approximately

thirty times higher than the aluminium content (Table 1) and, it has greater affinity for oxygen. Based on the value of activation energy in magnesium for grain boundary self diffusion (about 90 kJ $mol^{-1}$) [40], the diffusivity of Mg in the grain boundaries of the magnesium alloy was calculated to be 1.06 x10 $^{-12}$ $m^2/s$ at 200ºC. The obtained value is approximately similar to the diffusion coefficient for Al in magnesium, previously commented. Since differences between these two diffusion coefficients cannot justify the preferential diffusion of aluminium, additional effects accounting some non-equilibrium segregations solution should be invoked [41,42]

The SEM micrographs for the non-heated AZ31-O specimen show second phase particles dispersed evenly on the surface (Fig. 2a) and mainly composed of Mg, Al and Zn (Table 2), presumably the $(Al,Zn)_{49}Mg_{23}$ phase [43,44]. This result is attributed to the non-equilibrium solidification caused by the cooling rate of the casting process [45].

In the case of the AZ61-O specimens, it is apparent that the fraction of the surface covered by black areas increases significantly after 5 minutes of heating (Fig. 2d). In the commercial magnesium alloys tested in this work there seems to be a direct relationship between the formation of MgO on the AZ61-O specimen during the initial stages of the heating process and the degree of microstructural complexity of the surface upon which it forms. Fig. 14 shows a very significant presence of β intermetallic phase on the boundary of AZ61 (Fig. 14b) compared to its absence on AZ31 (Fig. 14a), suggesting that the two-

phase nature of the alloy may play a significant role in the early stages of oxide formation [46].

*4.2. Relationship between the chemistry of the oxide layers formed on the surface of magnesium alloys as a result of the heat treatment and their corrosion resistance in saline solutions.*

It seems likely that some of the differences that have been revealed in the composition and characteristics of the oxide layers formed on the surfaces of the AZ31-O and AZ61-O specimens as a result of the heat treatment may have an impact on their corrosion behaviour. As commented earlier, the more significant features that have been observed on the oxide layer, depending on the type of alloy and heat treatment time, have been (a) the aluminium enrichment of the surface of the AZ31-O alloy after prolonged heat treatment time and (b) the absence of similar enrichments in the AZ61-O alloy.

Electrochemical impedance results (Figs. 9 and 10) and hydrogen evolution versus time curves (Fig.11) have provided information on the effect of experimental variables on the corrosion resistance of the specimens tested. For times of more than 1 hour up to the end of the immersion test, it is clear the trend of the AZ31-O specimen heated for 20 and 60 minutes to present lower $R_t$ and higher corrosion rates than the other tested specimens for the same immersion times (Fig.9a and 10). Many studies mention the beneficial effect of Al [47-53], which may become the essential factor in determining the passivity of the surface, improving the resistance to local breakdown of the oxide and reducing the chance of chloride ions penetrating as far as the surface. In the

literature [54], it is presumed that the $Al_2O_3$ component forms a continuous skeletal structure in an amorphous matrix, so that the film properties become predominantly determined by the protective properties of $Al_2O_3$, very superior to that of $Mg(OH)_2$. Curiously in our study, an opposite effect seems to be observed. Comparing the corrosion data (Figs 9a, 10a and 11a) with the chemical composition determined by EDX (Fig 4) and XPS (Fig 6) on the surface of the oxide layers resulting from the heat treatment, one can clearly see a tendency towards an increase in the corrosion rate (Fig.10a) values and an in the hydrogen volumes evolved (Fig. 11a) as the Al/(Al+Mg) ratio increases (Figs 4 and 6). This correspondence suggests an influence of the said enrichment in aluminium oxide/hydroxide of the surface of oxide layer as a result of the heat treatment on the corrosion process in posterior immersion in 0.6 M NaCl. Although the presence of the $Al_2O_3$ component can serve as diffusion barrier in compact scale, it seems likely that the aluminium surface enrichment observed in our study after the heating process had a heterogeneous island structure without any special effect for corrosion protection [16]. The atomic ratio Al/(Mg+Al) determined by EDX on the surface of the AZ31-O alloy after 20 and 60 minutes of heating reached values of 4% and 6%, which are two or three times higher than those non-heated or heated for 5 minutes specimens (Fig.4). It is probable that this surface enrichment in aluminium over prolonged heating periods contributes to a significant decrease in the aluminium content of the primary α-Mg matrix in the region close to the sheet surface. According with Song et al [5] and Zhou et al [8], it may be speculated that the development of an alloy layer of low Al content immediately

beneath the oxide film makes the α matrix more active causing an increase in the corrosion rate.

Finally, in the case of the AZ61-O specimens, it is interesting to note the absence of significant variations in the corrosion rate, (Fig.10b) or in the volumes of hydrogen evolved (Fig. 11b) as a function of the heating time, where the EDX and XPS analyses (Figs.4 and 6,respectively) have revealed Al contents on the heated specimens similar to those observed on the non-heated alloy or in the bulk alloy (Table 1). This fact tends to support the idea that the aluminium incorporation in the magnesium oxide film that covers the surface of the magnesium alloys after the heat treatment plays a fundamental part in the observed corrosion rate.

## 5. Conclusions

SEM/EDX and XPS analyses have revealed notable differences in the oxide films formed on the surface of AZ31 and AZ61 alloys in as-received condition as a result of their heating in air at a temperature of 200°C for a time of 5 minutes to 1 hour. SEM and EDX analyses shows a larger fraction of the AZ31 alloy surface covered by precipitates, mainly composed by a mixture of $Al_2O_3$ and ZnO, than the AZ61 alloy surface. XPS analysis has revealed considerable superficial aluminium species enrichment of the AZ31 alloy owing to the heat treatment. Close to four times higher aluminium oxide contents have been found in these layers compared to the bulk content. Curiously, this phenomenon has not been detected in the AZ61 alloy subjected to identical treatment, which has higher aluminium content in the bulk composition

It seems likely that the heterogeneous structure associated with the second-phase played a decisive role in the enrichment phenomenon. The practically nil presence of β-phase on the AZ31 alloy favours the diffusion of aluminium atoms along the grain boundaries towards the outer surface, where they precipitate in the form of $Al_2O_3$. This result contrast with the presence of β-phase on the AZ61 alloy, preferentially along the grain boundaries, which may act as a barrier for diffusion of aluminium towards the outermost surface through the heating treatment.

EIS measurements in the interval of between 1 h and 28 days of immersion in 0.6M NaCl solution have allowed to relate the chemical composition of the oxide films formed as a result of the heating treatment with the corrosion resistance of the alloys. It is to point out the notable increase in corrosion rate of

the AZ31 alloy after 20 or 60 minutes of heat treatment compared to same alloy non-treated or only treated for 5 minutes. In contrast, no significant changes have been observed in the case of the heat treated AZ61 alloy

**Acknowledgment**

We wish to express our gratitude to Prof. S. Feliu for several clarifying and stimulating discussions during the course of this work. Also, the authors gratefully acknowledge the financial support for this work from the Ministry of Science and Innovation of Spain (MAT 2009-13530)

## References

[1] M.C. Zhao, M. Liu, G.L. Song, A. Atrens, Influence of the beta-phase morphology on the corrosion of the Mg alloy AZ91, Corros. Sci. 50 (2008) 1939-1953.

[2] M.C. Zhao, M. Liu, G.L. Song, A. Atrens, Influence of homogenization annealing of AZ91 on mechanical properties and corrosion behavior, Adv. Eng. Mater. 10 (2008) 93-103.

[3] C.L. Liu, Y.C. Xin, G.Y. Tang, P.K. Chu, Influence of heat treatment on degradation behavior of bio-degradable die-cast AZ63 magnesium alloy in simulated body fluid, Mater. Sci. Eng., A 456 (2007) 350-357.

[4] T. Beldjoudi, C. Fiaud, L. Robbiola, Influence of homogenization and artificial aging heat-treatments on corrosion behavior of Mg-Al alloys, Corrosion 49 (1993) 738-745.

[5] G.L. Song, A.L. Bowles, D.H. StJohn, Corrosion resistance of aged die cast magnesium alloy AZ91D, Mater. Sci. Eng., A 366 (2004) 74-86.

[6] N.N. Aung, W. Zhou, Effect of heat treatment on corrosion and electrochemical behaviour of AZ91D magnesium alloy, J. Appl. Electrochem. 32 (2002) 1397-1401.

[7] J.D. Majumdar, U. Bhattacharyya, A. Biswas, I. Manna, Studies on thermal oxidation of Mg-alloy (AZ91) for improving corrosion and wear resistance, Surf. Coat. Technol. 202 (2008) 3638-3642.

[8] W. Zhou, T. Shen, N.N. Aung, Effect of heat treatment on corrosion behaviour of magnesium alloy AZ91D in simulated body fluid, Corros. Sci. 52 (2010) 1035-1041.

[9] L.Q. Zhu, W.P. Li, D.D. Shan, Effects of low temperature thermal treatment on zinc and/or tin plated coatings of AZ91D magnesium alloy, Surf. Coat. Technol. 201 (2006) 2768-2775.

[10] H.Y. Hsiao, P. Chung, W.T. Tsai, Baking treatment effect on materials characteristics and electrochemical behavior of anodic film formed on AZ91D magnesium alloy, Corros. Sci. 49 (2007) 781-793.

[11] E. Aghion, N. Lulu, The effect of skin characteristics on the environmental behavior of die cast AZ91 magnesium alloy, J. Mater. Sci. 44 (2009) 4279-4285.

[12] G. L. Song, A. Atrens, M. Dargusch, Influence of microstructure on the corrosion of diecast AZ91D, Corros. Sci. 41 (1999) 249-273.

[13] B.L. Yu, J.Y. Uan, Correlating the microstructure of the die-chill skin and the corrosion properties for a hot-chamber die-cast AZ91D magnesium alloy, Mater. Trans. A. 36A (2005) 2245-2252.

[14] W. Zhang, S. Jin, E. Ghali, R. Tremblay, Skin and bulk corrosion properties of die cast and thixocast AZ91D magnesium alloy in 0.05M NaCl solution, Can. Metall. Q. 45 (2006) 181-188.

[15] G.L. Song, Z.Q. Xu, The surface, microstructure and corrosion of magnesium alloy AZ31 sheet, Electrochim. Acta 55 (2010) 4148-4161.

[16] S. Feliu Jr., C. Maffiotte, A. Samaniego, J.C. Galvan, V. Barranco, Effect of the chemistry and structure of the native oxide surface film on the corrosion properties of commercial AZ31 and AZ61 alloys, Appl. Surf. Sci. 257 (2011) 8558-8658.

[17] M.F. Lopez, J.A. Jimenez, A. Gutierrez, XPS characterization of surface modified titanium alloys for use as biomaterials, Vacuum 85 (2011) 1076-1079.

[18] S. Feliu Jr., C. Maffiotte, A. Samaniego, J.C. Galvan, V. Barranco, Effect of naturally formed oxide films and other variables in the early stages of Mg-alloy corrosion in NaCl solution, Electrochim. Acta 56 (2011) 4454-4565.

[19] L.P.H. Jeurgens, M.S. Vinodh, E.J. Mittemeijer, Initial oxide-film growth on Mg-based MgAl alloys at room temperature, Acta Mater. 56 (2008) 4621-4634.

[20] F. Czerwinski, The oxidation behaviour of an AZ91D magnesium alloy at high temperatures, Acta Mater. 50 (2002) 2639-2654.

[21] C.D. Wagner, L.E. Davis, M.V. Zeller, J.A. Taylor, R.H. Raymond, L.H. Gale, Empirical atomic sensitivity factors for quantitative-analysis by electron-spectroscopy for chemical-analysis, Surf. Interface Anal. 3 (1981) 211-225.

[22] G. Song, A. Atrens, D. Stjohn, J. Naim, Y. Li, The electrochemical corrosion of pure magnesium in 1 N NaCl, Corros. Sci. 39 (1997) 855-875.

[23] G.L. Song, A. Atrens, X.L. Wu, B. Zhang, Corrosion behaviour of AZ21, AZ501 and AZ91 in sodium chloride, Corros. Sci. 40 (1998) 1769-1791

[24] H.B. Yao, Y. Li, A.T.S. Wee, An XPS investigation of the oxidation/corrosion of melt-spun Mg, Appl. Surf. Sci. 158 (2000) 112–119.

[25] V. Fournier, P. Marcus, I. Olefjord, Oxidation of magnesium, Surf. Interface Anal. 34 (2002) 494-497.

[26] J. Kim, K.C. Wong, P.C. Wong, S.A. Kunlich, J.B. Metson, K.A.R. Mitchell, Characterization of AZ91 magnesium alloy and organosilane adsorption on its surface, Appl. Surf. Sci. 253 (2007) 4197-4207.

[27] N.C. Hosking, M.A. Ström, P.H. Shipway, C.D. Rudd, Corrosion resistance of zinc-magnesium coated steel, Corros. Sci. 49 (2007) 3669-3695.

[28] M. Liu, P. Shmutz, S. Zanna, A. Seyeux, H. Ardelean, G. Song, A. Atrens, P. Marcus, Electrochemical reactivity, surface composition and corrosion mechanisms of the complex metallic alloy $Al_3Mg_2$, Corros. Sci. 52 (2010) 562-578.

[29] M Liu, S Zanna, H Ardelean, I Frateur, P Schmutz, G Song, A Atrens, P Marcus, A first quantitative XPS study of the surface films formed, by exposure to water, on Mg and on the Mg-Al intermetallics: Al3Mg2 and Mg17Al12, Corros. Sci. 51 (2009) 1115-1127.

[30] N. Pebere, C. Riera, F. Dabosi, Investigation of magnesium corrosion in aerated sodium-sulfate solution by electrochemical impedance spectroscopy, Electrochim. Acta, 35 (1990) 555-561.

[31] G.I. Makar, J. Kruger, Corrosion studies of rapidly solidified magnesium alloys, J. Electrochem. Soc. 137 (1990) 414-421.

[32] S. Mathieu, C. Rapin, J. Hazan, P. Steinmetz, Corrosion behaviour of high pressure die-cast and semi-solid cast AZ91D alloys, Corros. Sci. 44 (2002) 2737-2756.

[33] M. Stern, A. L. Geary, Electrochemical polarization1. A theoretical analysis of the shape of polarization curves, J. Electrochem. Soc. 104 (1957) 56-63.

[34] C. Lea, C. Molinari, Magnesium diffusion, surface segregation and oxidation in Al-Mg alloys, J. Mater. Sci. 19 (1984). 2336-2352.

[35] A. Samaniego, I. Llorente, S. Feliu Jr., Combined effect of composition and surface condition on corrosion behaviour of magnesium alloys AZ31 and AZ61, Corros. Sci., 68 (2012) 66-71.

[36] G. Moreau , J.A. Cornet , D. Calais, Acceleration de la diffusion chimique sous irradiation dans le systeme aluminium-magnesium, J. Nucl.Mater. 38 (1971) 197-202.

[37] K.N. Braszczynska-Malik. Discontinuous and continuous precipitation in magnesium-aluminium type alloys, J. Alloys Compd 477 (2009) 870-876.

[38] B. Kim, B. Kang, Y. Park, I. Park, Influence of Pd addition on the creep behavior of AZ61 magnesium alloy, Mater. Sci. Eng., A 528 (2011) 5747-5753.

[39] A. Srinivasan, J. Swaminathan, M.K. Gunjan, U.T.S. Pillai, B.C. Pai, Effect of intermetallic phases on the creep behavior of AZ91 magnesium alloy, Mater. Sci. Eng., A 527 (2010) 1395-1403.

[40] H.J Frost, M.F Ashby Deformation Mechanism Maps, Pergamon Press, Oxford (1983), p. 44.

[41] Ya.B Unigovski, E.M Gutman, Surface morphology of a die-cast Mg alloy, Appl. Surf. Sci. 153 (1999) 47-52.

[42] P. Bassani, E. Gariboldi, A. Tuissi, Calorimetric analysis of AM60 magnesium alloys, J. Therm. Anal. Calorim. 80 (2003) 739-747.

[43] G.F. Vander Voort (Ed.), Metallography and Microstructures, vol. 9ASM International, Materials Park, OH (2004).

[44] M. Masoumi, F. Zarandi, M. Pekguleryuz, Microstructure and texture studies on twin-roll cast AZ31 (Mg–3 wt.%Al–1 wt.%Zn) alloy and the effect of thermomechanical processing, Mater. Sci. Eng., A 528 (2011) 1268-1279.

[45] M.S. Dargusch, K. Pettersen, K. Nogita, M.D. Nave and G.L. Dunlop, The Effect of Aluminium Content on the Mechanical Properties and Microstructure of Die Cast Binary Magnesium-Aluminium Alloys, Mater. Trans., JIM 47 (2006) 977-982.

[46] S.J. Splinter, N.S. McIntyre, The initial interaction of water-vapor with mg-al alloy surfaces at room-temperature, Surf. Sci. 314 (1994) 157-171

[47] S. Feliu Jr., M.C. Merino, R. Arrabal, A.E. Coy, E. Matykina, XPS study of the effect of aluminium on the atmospheric corrosion of the AZ31 magnesium alloys, Surf. Interface Anal. 41 (2009) 143-150.

[48] R. Lindstrom, J.E. Svensson, L.G. Johansson, The influence of carbon dioxide on the atmospheric corrosion of some magnesium alloys in the presence of NaCl, J. Electrochem. Soc. 149 (2002) B 103 - B 107.

[49] M. Liu, P.J. Uggowitzer, A.V. Nagasekhar, P. Schmutz, M. Easton, G. L. Song, A. Atrens, Calculated phase diagrams and the corrosion of die-cast Mg-Al alloys, Corros. Sci. 51 (2009) 602-619.

[50] J.H. Nordlien, K. Nisancioglu, S. Ono. N. Masuko, Morphology and structure of oxide films formed on MgAl alloys by exposure to air and water, J. Electrochem. Soc. 143 (1996) 2564-2572.

[51] A. Pardo, M.C. Merino, A.E. Coy, R. Arrabal, F. Viejo, E. Matykina, Corrosion behaviour of magnesium/aluminium alloys in 3.5 wt% NaCl, Corros. Sci. 50 (2008) 823-834.

[52] M. Jönsson, D. Persson, R. Gubner, The initial steps of atmospheric corrosion on magnesium alloy AZ91D, J. Electrochem. Soc. 154 (2007) C684-C691.

[53] N. Hara, Y. Kobayashi, D. Kagaya, N. Akao, Formation and breakdown of surface films on magnesium and its alloys in aqueous solutions, Corros. Sci. 49 (2007) 166-175.

[54] J.H.Nordlien, S. Ono, N. Masuko, K. Nisancioglu**,** A TEM investigation of naturally formed oxide films on pure magnesium, Corros. Sci. 39 (1997) 1397-1414.

FIGURE CAPTIONS

**Fig. 1.** Evolution of weight gain values obtained in the AZ31 and AZ61 in as-received conditions alloys as a function of the time of heating at 200ºC in air compared with those of the same alloys in polished condition.

**Fig. 2.**. SEM surface morphologies for AZ31 (a, c, e, g) and AZ61 magnesium in as-received conditions alloys (b, d, f, h) non-heated (a, b) and heated for 5 min (c, d), 20 min (e, f) and 60 minutes (g,h) at 200ºC in air, respectively.

**Fig. 3.**. Micrograph illustrating locations of points for EDX spot analysis of the AZ31 magnesium in as-received condition alloy heated for 60 min at 200ºC in air. Spectrum 1, 2, 3 and 4 (white oxide nodules) and Spectrum 5 and 6 (Dark layer).

**Fig. 4.**. Variation in the Al/(Al+Mg) x 100 atomic ratio of the dark layer obtained by EDX on the surface of the AZ31-O and AZ61-O specimens as a function of the time of heating.

**Fig. 5.**. Variation in the Oxygen (a), Magnesium (b), Aluminium (c) and Zinc (d) atomic percentages obtained by XPS on the surface of the AZ31-O and AZ61-O specimens as a function of the time of heating.

**Fig. 6.**. Variation in the Al/(Al+Mg) x 100 atomic ratio obtained by XPS on the surface of the AZ31-O and AZ61-O specimens as a function of the time of heating.

**Fig. 7.**. High resolution O1s (a), Mg2p (b), Al2s (c) and $Zn2p_{3/2}$ (d) XPS peaks obtained by XPS on the surface of the AZ31 alloy after 5 minutes of heating.

**Fig. 8.**. Variation in Nyquist plot for AZ31-O and AZ61-O specimens with immersion time (hours or days on the *Y*-axis) and with times of heating.

**Fig. 9.**. Variation in $R_t$ values as a function of the time of heating and alloy type over 28 days immersion in 0.6M NaCl.

**Fig. 10.**. . Variation in corrosion rates (mm/y) obtained from EIS as a function of the time of heating and alloy type over 28 days immersion in 0.6M NaCl.

**Fig. 11.** Variation in $H_2$ evolution volume values as a function of the times of heating and alloy type over 14 days immersion in 0.6M NaCl.

**Fig. 12.** Representative macroscopic surface appearance of corroded AZ31 specimens after 14 days of immersion in NaCl 0.6M and after corrosion product removal. (a) non-heated alloy and (b) AZ31 alloy heated for 60 minutes at 200ºC in air.

**Fig. 13.** AFM images of the surfaces in the original (O) and polished (P) surface conditions for: (a) AZ31 alloy and (b) AZ61 alloy.

**Fig.14.** SEM micrographs: (a) AZ31 alloy and (b) AZ61 alloy.

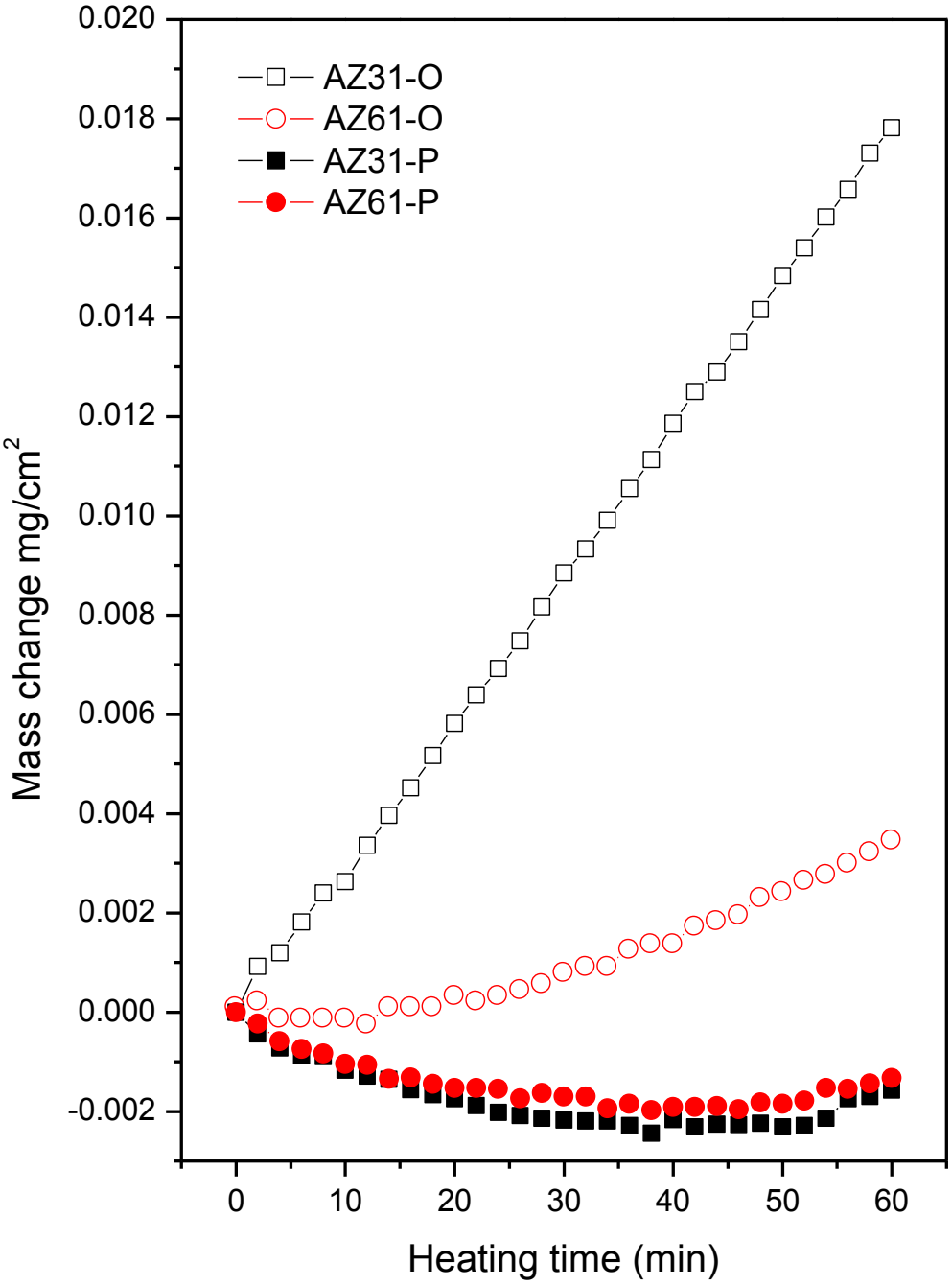
AZ31-O
AZ61-O
AZ31-P
AZ61-P
Mass change mg/cm2
Heating time (min)
0.020
0.018
0.016
0.014
0.012
0.010
0.008
0.006
0.004
0.002
0.000
-0.002
0
10
20
30
40
50
60

**Fig. 1.**

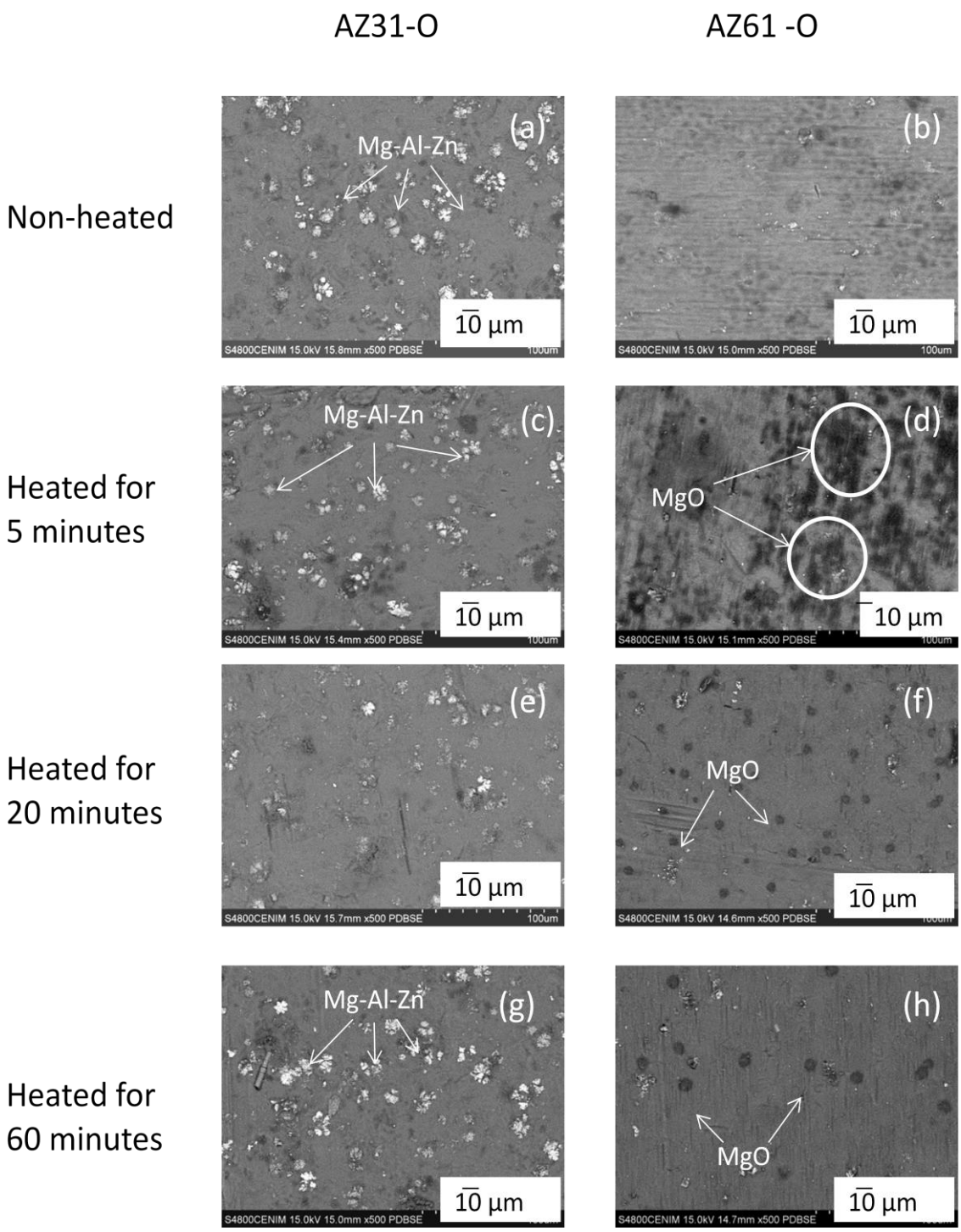
AZ31-O
AZ61 -O
Non-heated
Heated for 5 minutes
Heated for 20 minutes
Heated for 60 minutes
Mg-Al-Zn
MgO
(a)
(b)
(c)
(d)
(e)
(f)
(g)
(h)
10 µm

**Fig. 2.**.

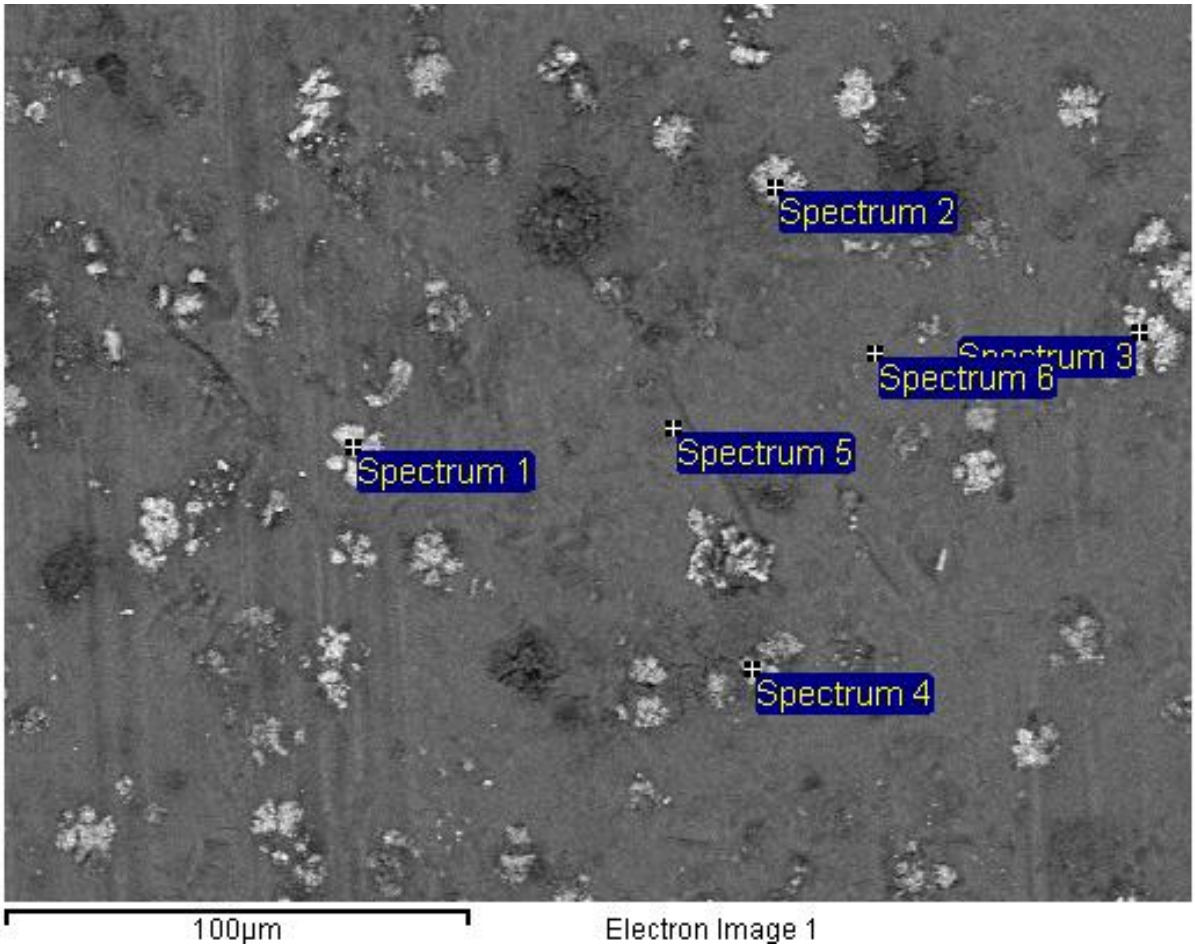
Spectrum 2
Spectrum 3
Spectrum 6
Spectrum 5
Spectrum 1
Spectrum 4
100µm
Electron Image 1

**Fig. 3.**.

.

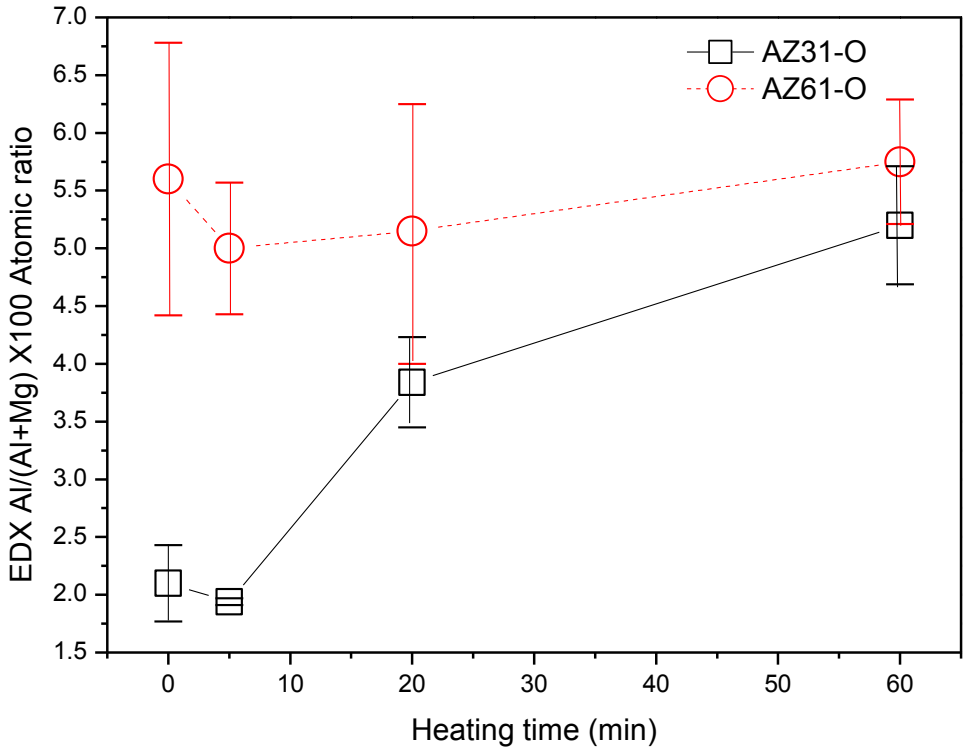
AZ31-O
AZ61-O
EDX Al/(Al+Mg) X100 Atomic ratio
Heating time (min)
7.0
6.5
6.0
5.5
5.0
4.5
4.0
3.5
3.0
2.5
2.0
1.5
0
10
20
30
40
50
60

**Fig. 4.**.

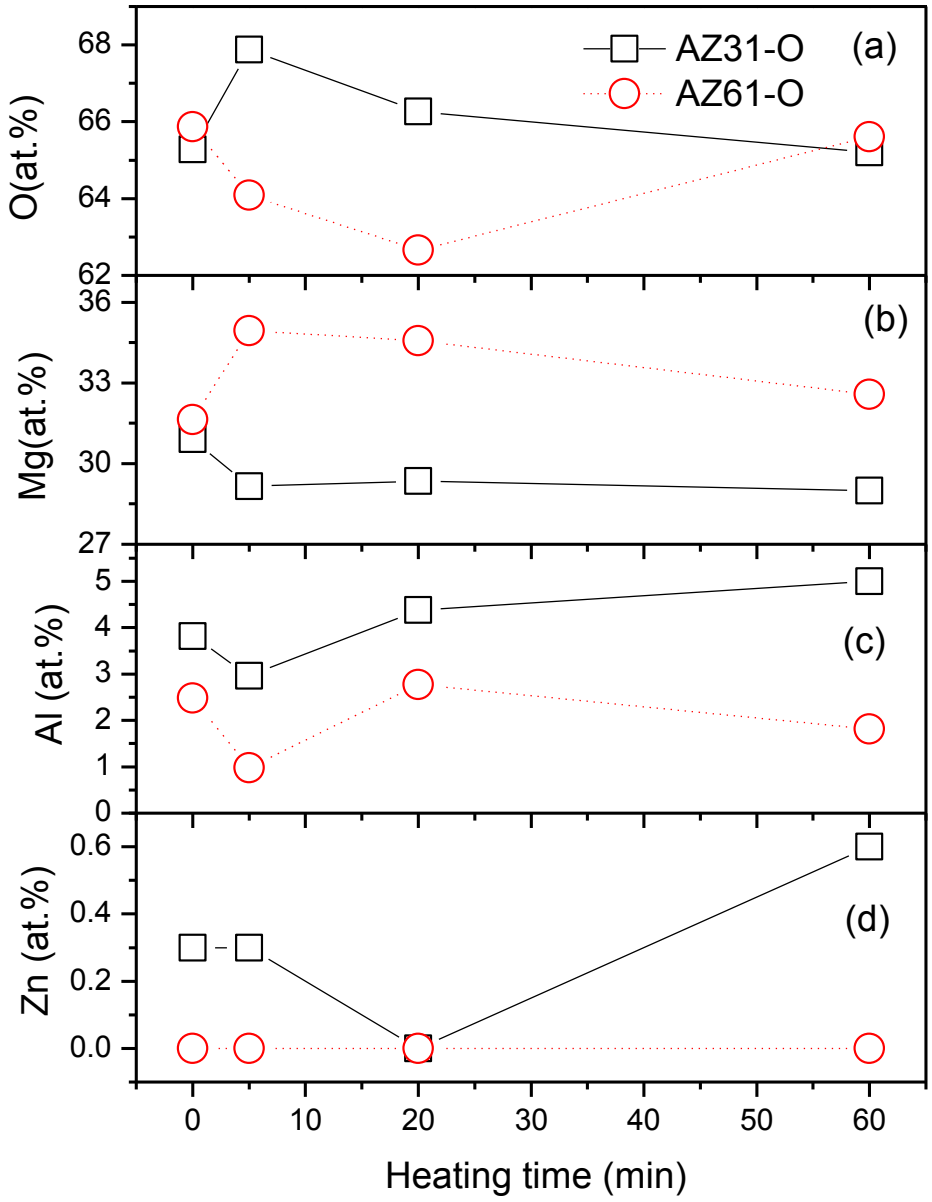
AZ31-O
AZ61-O
(a)
(b)
(c)
(d)
O(at.%)
Mg(at.%)
Al (at.%)
Zn (at.%)
Heating time (min)
68
66
64
62
36
33
30
27
5
4
3
2
1
0
0.6
0.4
0.2
0.0
0
10
20
30
40
50
60

**Fig. 5.**.

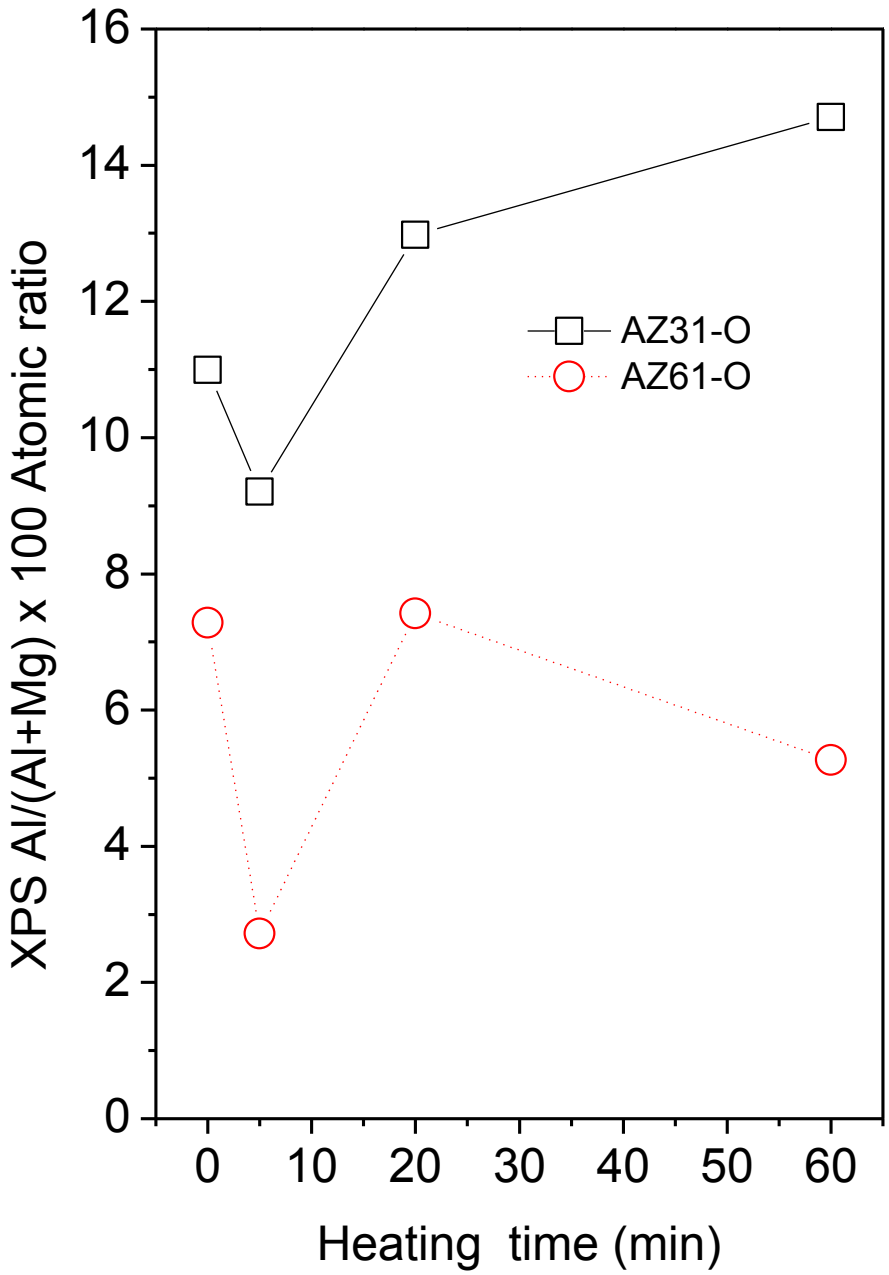
16
14
12
10
8
6
4
2
0
XPS Al/(Al+Mg) x 100 Atomic ratio
0
10
20
30
40
50
60
Heating time (min)
AZ31-O
AZ61-O

**Fig. 6.**.

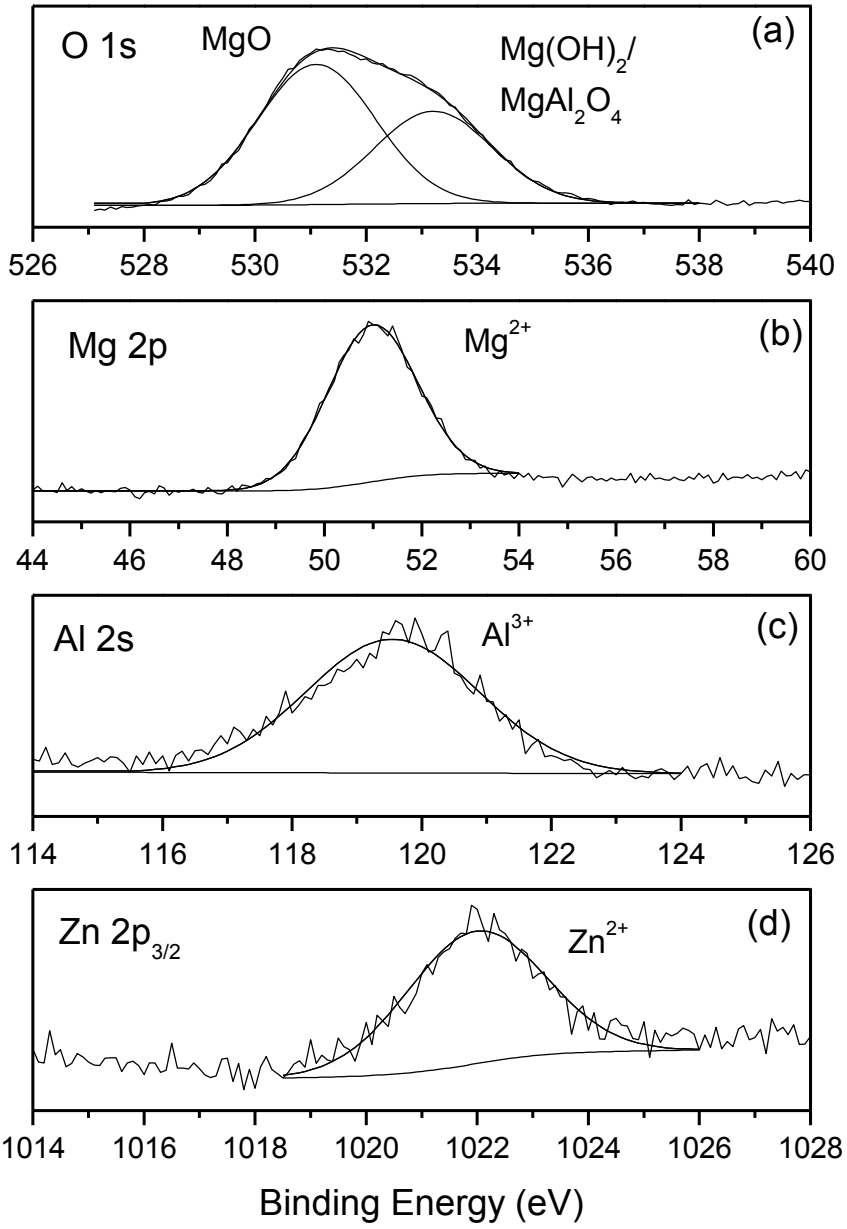
O 1s
MgO
Mg(OH)2/
MgAl2O4
(a)
526
528
530
532
534
536
538
540
Mg 2p
Mg2+
(b)
44
46
48
50
52
54
56
58
60
Al 2s
Al3+
(c)
114
116
118
120
122
124
126
Zn 2p3/2
Zn2+
(d)
1014
1016
1018
1020
1022
1024
1026
1028
Binding Energy (eV)

**Fig. 7.**

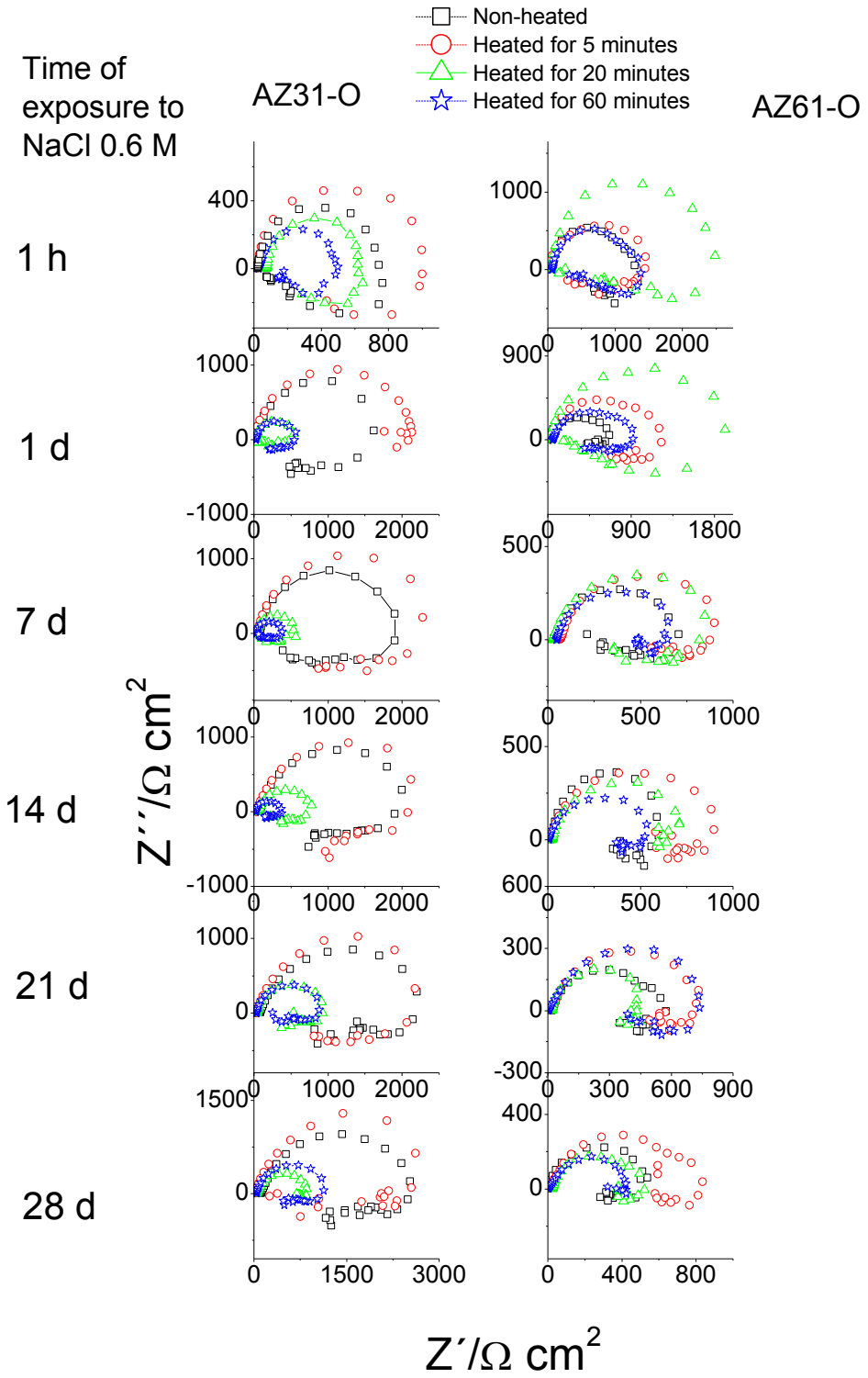
Non-heated
Heated for 5 minutes
Heated for 20 minutes
Heated for 60 minutes
Time of exposure to NaCl 0.6 M
AZ31-O
AZ61-O
1 h
1 d
7 d
14 d
21 d
28 d
Z´´/Ω cm2
Z´/Ω cm2

**Fig. 8.**.

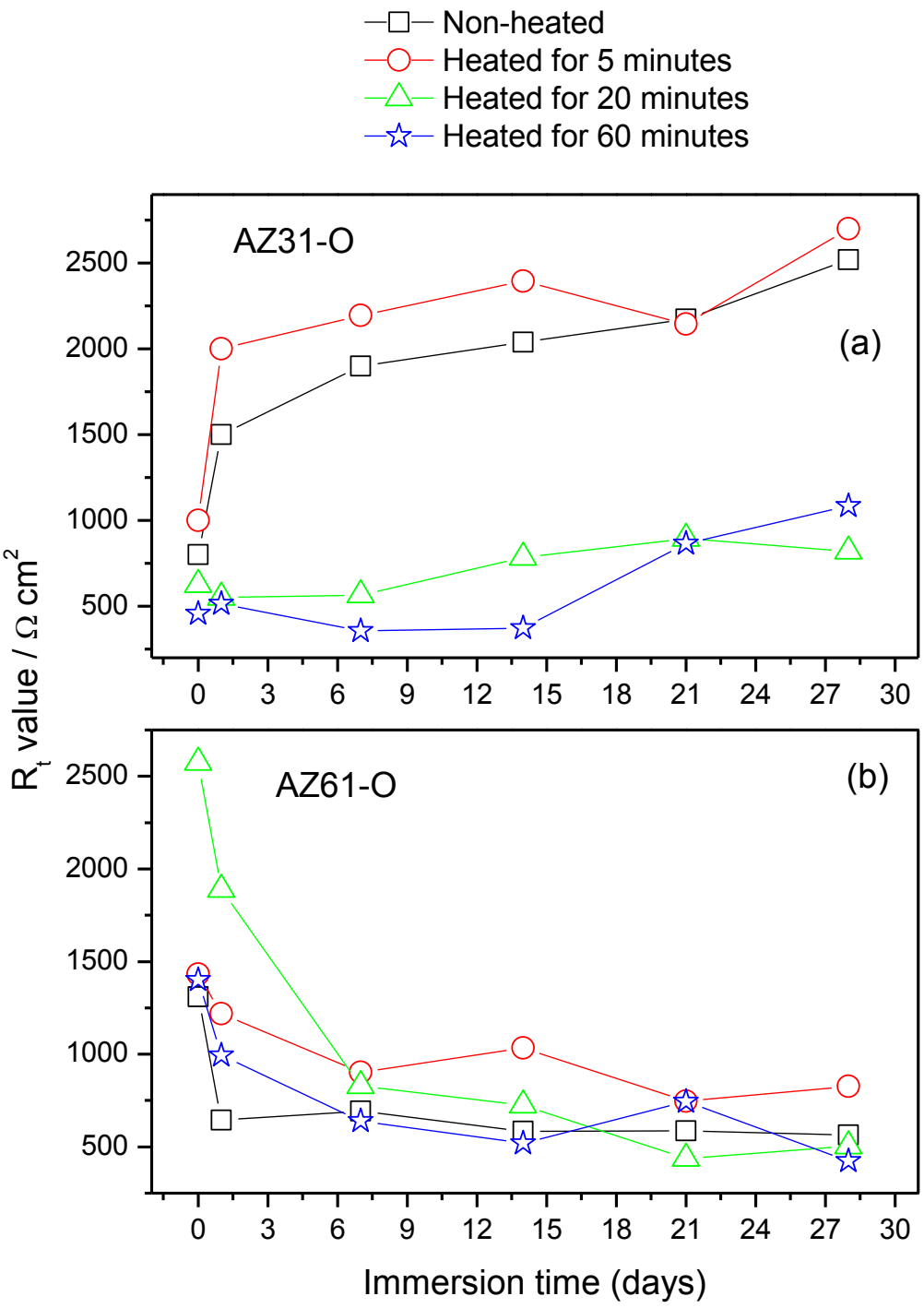
Non-heated
Heated for 5 minutes
Heated for 20 minutes
Heated for 60 minutes
AZ31-O
(a)
AZ61-O
(b)
$R_t$ value / Ω cm$^2$
Immersion time (days)
2500
2000
1500
1000
500
0
3
6
9
12
15
18
21
24
27
30

**Fig. 9.**.

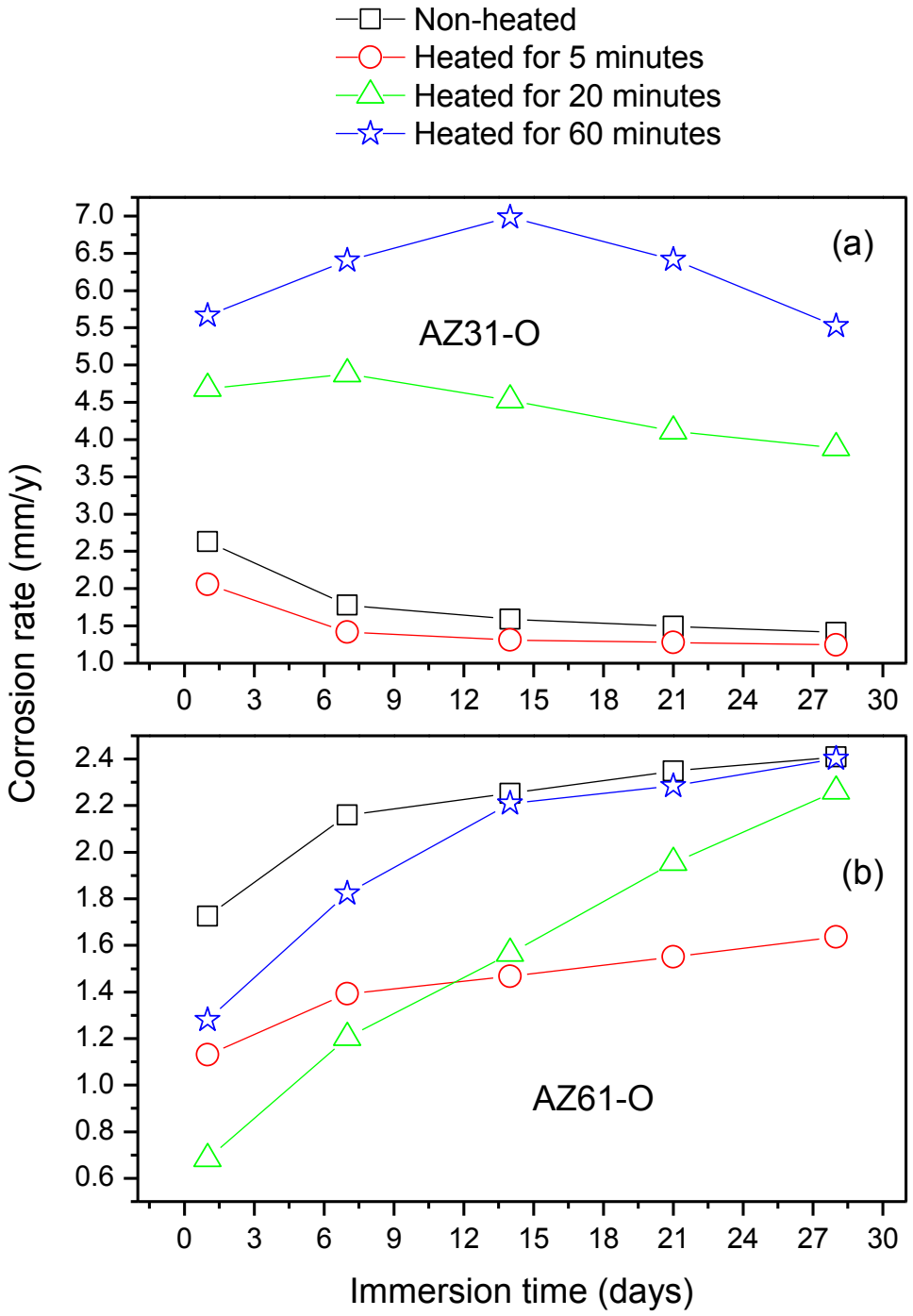
Non-heated
Heated for 5 minutes
Heated for 20 minutes
Heated for 60 minutes
(a)
AZ31-O
(b)
AZ61-O
Corrosion rate (mm/y)
Immersion time (days)

**Fig. 10.**.

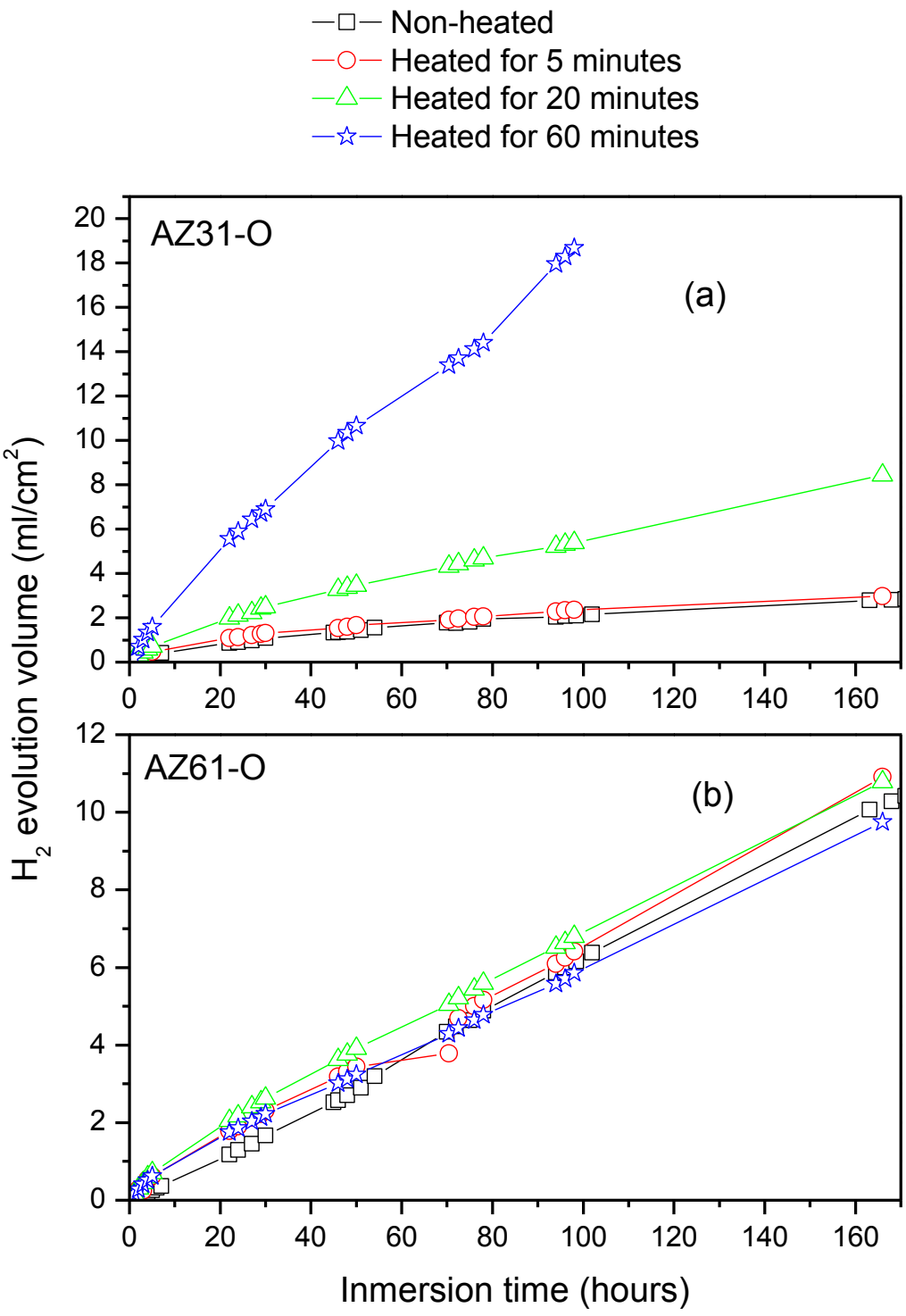
Non-heated
Heated for 5 minutes
Heated for 20 minutes
Heated for 60 minutes
AZ31-O
(a)
AZ61-O
(b)
H2 evolution volume (ml/cm2)
Inmersion time (hours)
0
20
40
60
80
100
120
140
160
0
2
4
6
8
10
12
14
16
18
20

**Fig. 11.**

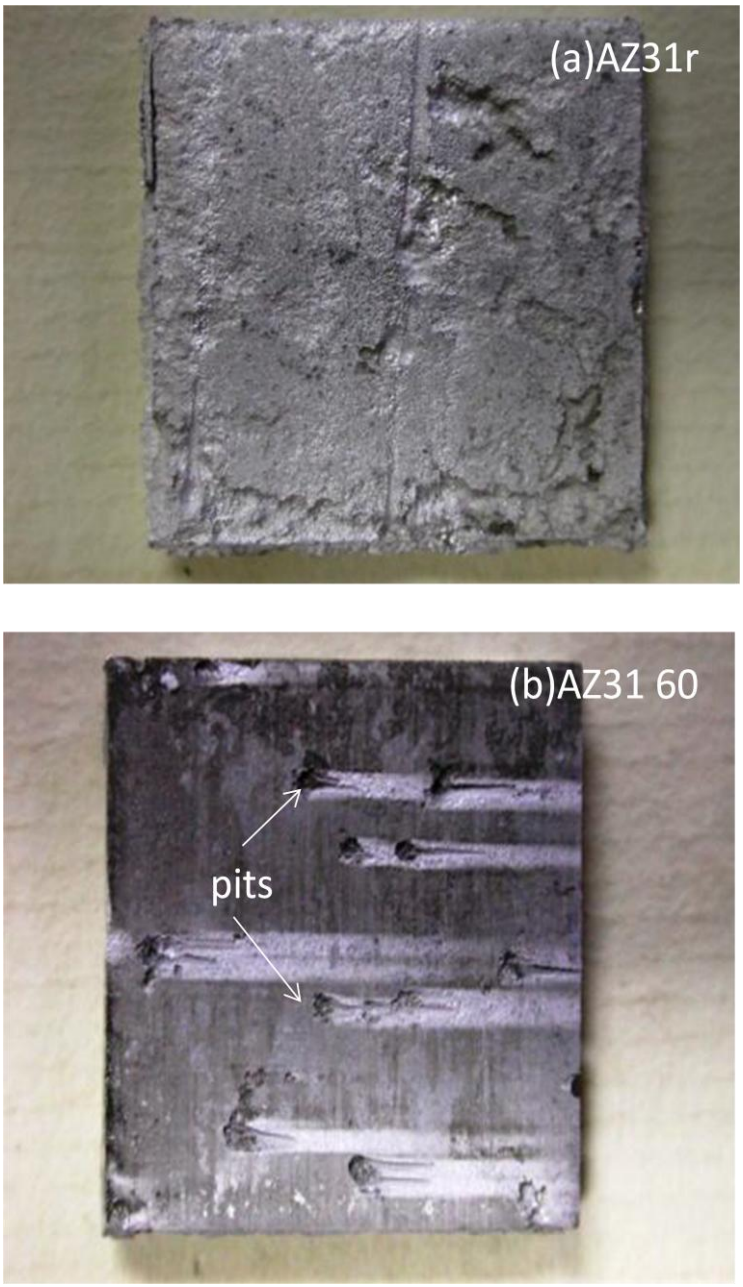


**Fig. 12.**

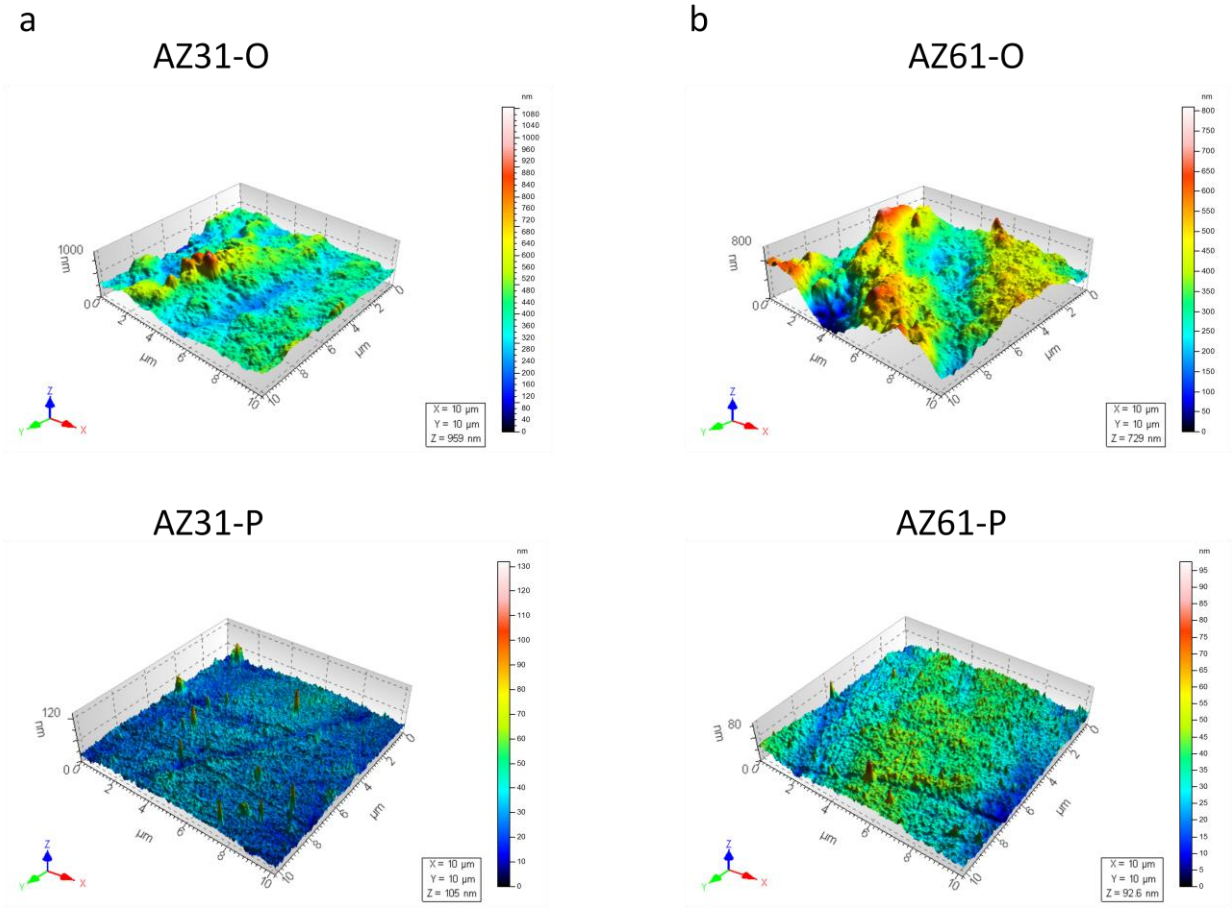


**Fig. 13.**.

AZ31 alloy

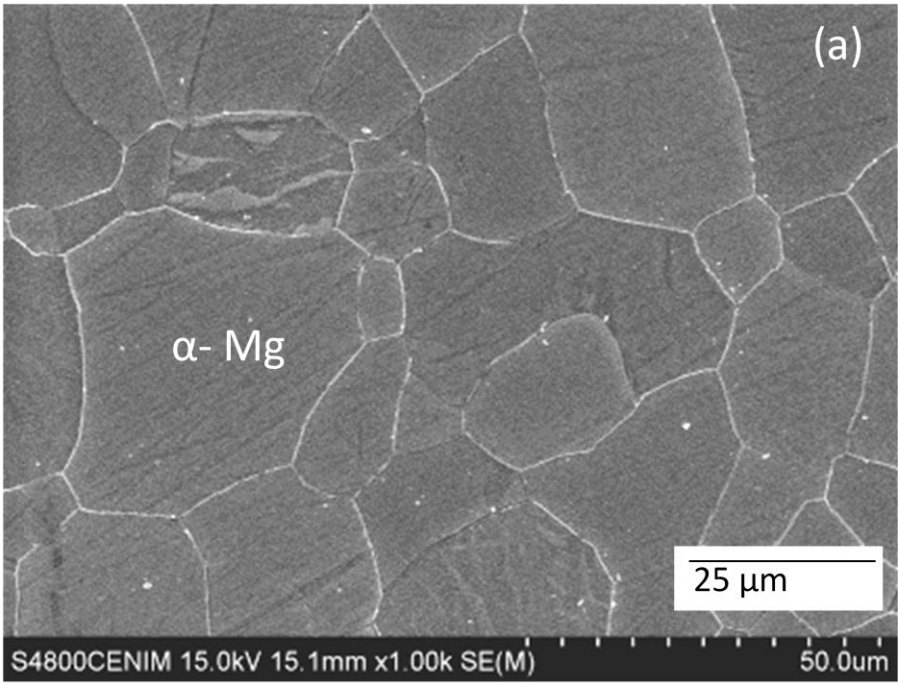


AZ61 alloy

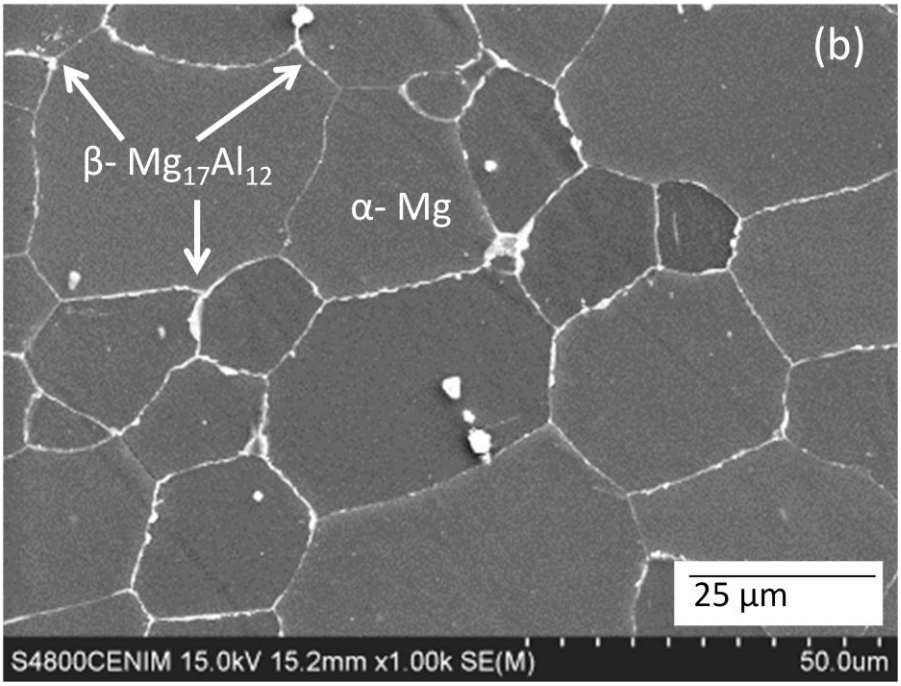


**Fig.14.**

**Table 1**. Chemical composition of AZ31 and AZ61 alloys (wt. %).

| Alloy | Al | Zn | Mn | Si | Fe | Ca | Mg |
|---|---|---|---|---|---|---|---|
| AZ31 | 3.1 | 0.73 | 0.25 | 0.02 | 0.005 | 0.0014 | Bal. |
| AZ61 | 6.2 | 0.74 | 0.23 | 0.04 | 0.004 | 0.0013 | Bal. |

**Table 2.** Measurements of atomic composition by EDX on the surface of the AZ31-O heated for 60 minutes.

| | White spots | Dark layer |
|---|---|---|
| Element | EDX (Average values from spectrum 1, 2, 3 and 4) (at%) | EDX[a] (Average values from spectrum 5 and 6) (at%) |
| O | 37.28 ± 5.12 | 13.27 ± 0.11 |
| Mg | 20.26 ± 7.68 | 81.73 ± 0.45 |
| Al | 13.86 ± 5.88 | 3.91 ± 0.43 |
| Mn | 1.75 ± 0.16 | 0.02 ± 0.03 |
| Zn | 26.49 ± 5.70 | 1.02 ± 0.11 |
| Al/(Mg+Al)x100 | 41.39 ± 19.04 | 4.57 ± 0.50 |

**Table 3.** Roughness values obtained with atomic force microscope. The values are average of four determinations.

| SPECIMENS | RMS (nm) |
|---|---|
| ORIGINAL SURFACE | |
| AZ31 | 123.1 |
| AZ61 | 109.6 |
| AFTER POLISHING | |
| AZ31 | 7.0 |
| AZ61 | 8.4 |